



# Effectiveness and optimal design of fluid-viscous dampers for inter-storey isolated buildings

Marco Donà<sup>ab</sup>, Enrico Bernardi<sup>b</sup>, Alberto Zonta<sup>b</sup>, Massimiliano Minotto<sup>b</sup>, Francesca da Porto<sup>c</sup>, Ping Tan<sup>a</sup>

<sup>a</sup> Earthquake Engineering Research & Test Center, University of Guangzhou, Guang Yuan Zhong Rd. 248, 510405 (China)

<sup>b</sup> Dept. of Civil, Architectural and Environmental Engineering, University of Padova, Via Marzolo 9, 35131, Padova (IT)

<sup>c</sup> Dept. of Geosciences, University of Padova, Via Gradenigo 6, 35131, Padova (IT)

*Keywords: supplementary viscous damping, inter-storey isolation, multi-objective optimal design, genetic algorithm, fluid viscous damper (FVD), lead rubber bearing (LRB)*

## ABSTRACT

The use of fluid viscous dampers (FVDs) together with isolators is effective in reducing isolators' displacement while keeping low isolation stiffnesses: therefore, such a hybrid system is suitable for buildings with inter-storey isolation in order to limit P- $\Delta$  effects. However, previous studies regarding base isolation showed that the additional damping may also be detrimental, as it may increase inter-storey drifts and floor accelerations. Although the main effects of additional damping on base-isolated buildings are clear, the results obtained in previous studies are not always easy to compare as they are strongly influenced by initial hypotheses (e.g. damper features); in addition, the use of FVDs in buildings isolated at storey level has its own peculiarities, and the effectiveness of FVDs for the improved seismic performance of such structures has been investigated only recently.

First, this paper presents the main results of a recent study on the effectiveness of FVDs optimally designed for an inter-storey isolated building (case study); in this research, the FVDs are individually optimized for each accelerogram analysed by evaluating two competing objectives, i.e., the minimisation of both the isolators deflection and the superstructure total drift. Subsequently, as the optimal linearity degree of the FVDs proved to be strongly dependent on seismic input, making the design choice difficult, a more suitable multi-objective optimal design approach is proposed and applied to the same case study, which involves the use of surrogate response models.

## 1 INTRODUCTION

In the last few years, inter-storey isolation is becoming increasingly attractive for the seismic risk mitigation of both new and existing buildings, particularly in densely populated areas, also as alternative strategy to base isolation. As the name suggests, this technique consists of inserting the isolation layer between the storeys rather than at the base of structure. The reasons for applying this technique can be various and of different nature, such as: architectural concerns, feasibility of construction, and performance benefits.

Inter-storey isolation can greatly increase design flexibility in high-rise and multipurpose buildings, by separating them into two independent structural parts which can be designed with different shapes, materials and functions (Zhang et al. 2016, Liu et al. 2018); this represents both an advantage for architectural design and an important sustainable solution for densely populated areas (such as the main cities of the People's Republic of China), as it allows to realize,

for example, residential buildings on the top of large commercial buildings, with a considerable saving on land use.

In addition, although base isolation for multi-storey buildings is a well-known technique applied worldwide, it may sometimes encounter substantial economic and technical issues, which may limit its application. Firstly, installing base isolation is straightforward for new buildings, but becomes complicated and expensive for existing ones, since excavation and temporary support works are required. Instead, the installation of inter-storey isolation is relatively simple and generally less expensive and disruption-free; it may also allow extra storeys to be constructed on the top of existing buildings (if the vertical capacity allows this) without increasing the base shear forces, representing an innovative and realistic retrofitting approach (Chey et al. 2013, Zhou 2001). Secondly, base isolation is not as effective as inter-storey isolation for medium/high-rise buildings, because of the

flexibility and bending-type behaviour of such structures (Ziyaeifar et al. 1998). Lastly, moving the isolation layer to the upper storeys reduces the need for a seismic gap, which is necessary to accommodate the expected isolation displacement, but also expensive and sometimes impractical in densely-built urban areas.

This isolation strategy substantially converts the masses above the isolation layer into tuned masses, retaining their structural functions in addition to the control function; in other words, the principle of operation may be appropriately described as a nonconventional tuned mass damper (TMD) with a large mass ratio (Reggio et al. 2015).

Examples of this application to irregular high-rise buildings are the Idabashi First Building (Zhang et al. 2016) and the Shiodome Sumitomo Building (Tasaka et al. 2008) in Japan, two multipurpose buildings having substructure and superstructure with different structural shape. In China, this technique was used to isolate 50 buildings (seven- or nine-storey RC frames) in Beijing, built on top of a two-storey platform covering a very large ( $\sim 3 \text{ km}^2$ ) railway area (Zhou et al. 2004). Built relatively recently, in the National Taiwan University campus, the Civil Engineering Research Building is a nine-storey pre-cast RC structure with an inter-storey isolation system installed between the second and third floors, which also includes viscous dampers (Loh et al. 2013).

Although the importance of the subject is now fully recognized, the limited studies available on this topic, as well as the limited dissemination of this matter inside the seismic codes, limit the spread of this seismic mitigation strategy.

One of the main issues related to this innovative application, for which systematic studies are still missing, is the need of reducing the seismic drift between the structural parts separated by the isolation layer (superstructure and substructure), which is responsible for high stresses in the substructure. However, the main function of seismic isolation is to allow the isolated superstructure to move significantly, in order to ensure its good seismic performance (small floor accelerations and inter-storey drifts). Therefore, this requires careful optimization studies.

For this purpose, the use of supplemental dampers together with isolators (solution often adopted for base-isolated structures built near some active faults, is effective in reducing deflection of isolation layer. In this regard, many numerical studies were carried out to evaluate the effects of additional damping, provided by fluid viscous dampers (FVDs), in the case of base

isolation (Kelly 1999, Hall 1999, Providakis 2008, Fathi et al. 2015), and this research showed that this additional damping may also be detrimental, as inter-storey drifts and floor accelerations of the isolated structure may increase. However, the results are not always easy to compare, as they are strongly influenced by initial hypotheses (such as the FVD features); moreover, the use of FVDs in buildings isolated at storey level, rather than at the base, has its own peculiarities, and its effectiveness has been investigated only recently for a case study (Liu et al. 2018). Therefore, further research studies are needed to evaluate the effects of additional damping on the isolated superstructure, analysing a wide range of FVDs (various linearity degrees) and structural configurations.

In addition, suitable procedures for optimizing the FVD parameters (i.e., damping coefficient  $c$  and exponent  $\alpha$ ) are necessary to support the design phase.

First, this paper presents the main results of a recent research (Liu et al. 2018) about the effectiveness of optimal FVDs in improving the seismic response of a seven-floor building with natural and lead rubber bearings (NRBs and LRBs) placed between the second and third levels. In particular, in this case study, a direct multi-objective optimization procedure is implemented, which uses the NSGA-II genetic algorithm to individually optimize the FVD parameters for each earthquake analysed; what emerges from this study is that, in general, the linearity degree of FVD ( $\alpha$ ) is strongly dependent on the non-linear response of the structure and therefore on the specific accelerogram, making this approach not appropriate for design purposes (as it is not possible to average the  $\alpha$  values). Therefore, a different approach for the multi-objective optimal design of the FVDs is subsequently proposed and applied to the same case study, and the results compared with those of the previous direct method. This new approach involves the use of surrogate response models and proved to be more effective for design purposes.

## 2 CASE STUDY

### 2.1 Building model and dynamic solution

The building model examined in Liu et al. (2018) is shown in Figure 1a. It includes a two-floor substructure and a five-floor superstructure elevated above the storey-isolation system.

The isolated superstructure (including the isolation system) is very similar to an existing

base-isolated office building with an RC frame structure, whereas the substructure is ideal and was chosen, for the purposes of the study, with a different structural solution, as shown in Table 1. Indeed, the substructure masses are similar to those of the upper storeys, whereas the storey lateral stiffness of substructure is about three times higher than that of the first superstructure storey, and this represents the case of a lightweight substructure with a floor extension larger than that of the superstructure. Such irregular building, with an office or residential multi-storey RC building constructed over a wider commercial building of different material, is increasingly common in highly populated residential areas (as in China).

The elastic ( $k$ ) and post-elastic ( $rk$ ) stiffnesses of the isolation system, realized with LRBs and NRBs, are reported in Table 1 (post-elastic stiffness ratio  $r$  is 0.141, see also Liu et al. 2018).

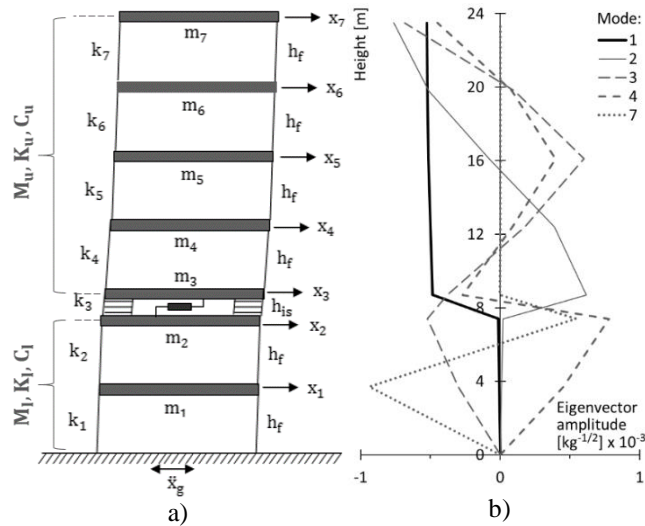


Figure 1. (a) Seven-storey building model with storey isolation; (b) modal shapes with post-elastic ( $rk$ ) stiffness.

Table 1. Stiffnesses and masses of building model.

Storey (inter-storey height: $h_f=3.7\text{m}$ , $h_{is}=1.3\text{m}$ )	1 <sup>st</sup>	2 <sup>nd</sup>	3 <sup>rd</sup>		4 <sup>th</sup>	5 <sup>th</sup>	6 <sup>th</sup>	7 <sup>th</sup>
			Elastic	Post-Elastic				
Stiffness (kN/mm)	1330	1140	$k=118.4$	$rk=16.7$	380	300	300	250
Mass (tons)	850	850	960	830	800	800	500	

Table 2. Results of modal analysis (post-elastic isolation stiffness) and structural damping ratios  $\zeta_i$  (Equation 5).

Mode	Angular frequency $\omega$ [rad/s]	Vibration period $T$ [s]	Modal contribution [%]	$\zeta_{l,i}$ due to substructure [%]	$\zeta_{u,i}$ due to superstructure [%]	$\zeta_{Tot,i}$ due to total structure (without LRBs and FVD) [%]
1	2.0	3.14	70.6	0.01	0.02	0.03
2	12.8	0.49	0.1	0.01	2.59	2.59
3	24.0	0.26	8.6	1.55	3.49	5.03
4	24.3	0.26	18.5	3.40	1.54	4.94
5	32.2	0.20	0.0	0.00	6.75	6.75
6	37.2	0.17	0.0	0.00	7.80	7.80
7	60.7	0.10	2.1	5.00	0.00	5.00

A generic FVD is then added to the isolation layer, the parameters of which are calculated in the next section, to obtain optimal design solutions.

Table 2 (left) and Figure 1b provide the main modal results, i.e. respectively, modal frequencies, periods and contributions, and modal shapes.

The dynamic equation governing the motion of such a building model for each time instant  $t$  is:

$$\mathbf{M}\ddot{\mathbf{x}}(t) + \mathbf{C}_{st}\dot{\mathbf{x}}(t) + \mathbf{K}_{st}\mathbf{x}(t) + \mathbf{r}_{is}F_{is}(t) + \mathbf{r}_{vd}F_{vd}(t) = -\mathbf{M}\ddot{\mathbf{u}}_g(t) \quad (1)$$

$\mathbf{x}(t)$ ,  $\dot{\mathbf{x}}(t)$ ,  $\ddot{\mathbf{x}}(t)$ , expressed as  $[x_1(t) \ x_2(t) \ \dots \ x_7(t)]^T$  and so on, are the vectors of the relative storey displacement, velocity and acceleration, with respect to the base of the building and represent the output of the dynamic equation.  $\ddot{\mathbf{u}}_g(t)$  is the acceleration time series of ground motion, and  $\mathbf{I}$  represents the unitary rigid displacement vector of the structure in the earthquake direction (i.e., identity vector in this case study).  $\mathbf{M}$ ,  $\mathbf{C}_{st}$  and  $\mathbf{K}_{st}$  are the matrices of mass, damping and stiffness of the building; in particular,  $\mathbf{C}_{st}$  and  $\mathbf{K}_{st}$  do not include the isolation layer and thus have the form:

$$\mathbf{K}_{st} = \begin{bmatrix} \mathbf{K}_l[2 \times 2] & \\ & \mathbf{K}_u[5 \times 5] \end{bmatrix}; \quad \mathbf{C}_{st} = \begin{bmatrix} \mathbf{C}_l[2 \times 2] & \\ & \mathbf{C}_u[5 \times 5] \end{bmatrix} \quad (2)$$

$l$  and  $u$  indicate the building lower and upper parts.

$\mathbf{K}_l$  and  $\mathbf{K}_u$  are directly obtained from the stiffness values of Table 1, whereas  $\mathbf{C}_l$  and  $\mathbf{C}_u$  are derived as in Equations 3 and 4, according to the Rayleigh and stiffness-proportional models, respectively.

$$\mathbf{C}_l = \alpha_l \mathbf{M}_l + \beta_l \mathbf{K}_l; \quad \alpha_l = 0.05 \cdot \frac{2\omega_3\omega_7}{\omega_3 + \omega_7}; \quad \beta_l = 0.05 \cdot \frac{2}{\omega_3 + \omega_7} \quad (3)$$

$$\mathbf{C}_u = \beta_u \mathbf{K}_u; \quad \beta_u = 0.05 \cdot \frac{2}{\omega_3} \quad (4)$$

Indeed, for this type of structures, a non-classical global damping model should be used (Ryan and Polanco 2008, Pant et al. 2013).

Rayleigh coefficients  $\alpha_l$  and  $\beta_l$  were calibrated by associating a damping ratio  $\zeta$  of 5% to the third and seventh mode frequencies (see Table 2), which define the significant vibrational range of the substructure. As regards  $\beta_u$ , a  $\zeta$  of 5% was associated to  $\omega_3$ , which is the first significant mode of superstructure; this leads to a slightly smaller damping with respect to the suggestion of Pant et al. (2013) of using, for base isolated buildings,  $\zeta=1\%$  at  $\omega_1$  (obtained with the post-elastic isolation stiffness). This is preferable considering that the stiffness-proportional damping model tends to suppress higher mode effects, which are more important in the case of storey isolation.

To verify the goodness of these choices, Table 2 (right) lists modal damping ratios  $\zeta_i$  due to the substructure [C<sub>s</sub>], superstructure [C<sub>u</sub>] and global structure [C<sub>st</sub>] without isolation system, calculated according to Equation 5 for classical damping (where  $\phi_i$  and  $\omega_i$  are the mode shape and angular frequency of mode  $i$ , respectively), thus neglecting the off-diagonal coupling terms (negligible) of the damping matrix expressed in modal coordinates.  $\zeta_i$  is about 5% for the main higher modes, whereas it is negligible (as expected) for the first mode, as well as the related structural deformation compared with that of the isolation layer.

$$\zeta_i = \frac{\phi_i^T C \phi_i}{2\omega_i \phi_i^T M \phi_i} \quad (5)$$

The contribution of the isolation layer is described by the last two addenda of Equation 1. The force of the isolation system  $F_{is}(t)$  is predicted with the Bouc-Wen model (Ismail et al. 2009):

$$F_{is}(t) = rkx(t) + (1-r)kd_y z(t) \quad (6)$$

$r$  and  $k$  are specified above (Table 1);  $d_y$  is the yielding displacement of the LRBs, equal to 7.8 mm in this case study.  $z(t)$  is a function which defines the hysteretic behaviour, and satisfy the non-linear first-order differential equation below:

$$\dot{z}(t) = (A\dot{x}(t) - \beta|\dot{x}(t)|z(t)|z(t)|^{\eta-1} - \gamma\dot{x}(t)|z(t)|^\eta) / d_y \quad (7)$$

$A$ ,  $\beta$ ,  $\gamma$  and  $\eta$  are non-dimensional parameters influencing the hysteretic loop shape (Ikhouane et al. 2007). In this case study,  $A=\beta=\gamma=1$  and  $\eta=2$  (for further information, see Liu et al. 2018).

The FVD force  $F_{vd}(t)$  is calculated as:

$$F_{vd}(t) = c|\dot{x}|^\alpha \text{sgn}(\dot{x}) \quad (8)$$

where  $c$  and  $\alpha$  are the damping coefficient and exponent, respectively.

Lastly,  $\mathbf{r}_{is}$  and  $\mathbf{r}_{vd}$  are the vectors needed to correctly place the contributions of isolators and damper in the matrix equation of motion:

$$\mathbf{r}_{is} = \mathbf{r}_{vd} = [0 \quad -1 \quad 1 \quad 0 \quad 0 \quad 0 \quad 0]^T \quad (9)$$

By introducing the state space vector  $\mathbf{q}(t)$ , Equation 1 can be solved as a first-order differential equation in state space:

$$\begin{aligned} \mathbf{q}(t) &= [\mathbf{x}^T(t) \quad \dot{\mathbf{x}}^T(t) \quad z(t)]^T \\ \dot{\mathbf{q}}(t) &= [\dot{\mathbf{x}}^T(t) \quad \ddot{\mathbf{x}}^T(t) \quad \dot{z}(t)]^T = \mathbf{f}(\mathbf{q}(t)) - \mathbf{B}\ddot{\mathbf{u}}_g(t) \end{aligned} \quad (10)$$

where:

$$\mathbf{f}(\mathbf{q}(t)) = \begin{bmatrix} \dot{\mathbf{x}}^T(t) \\ -\mathbf{M}^{-1}(\mathbf{C}_{st}\dot{\mathbf{x}}(t) + \mathbf{K}\mathbf{x}(t) + \mathbf{r}_{is}(1-r)kd_y z(t) + \mathbf{r}_{vd}F_{vd}(t)) \\ \frac{1}{d_y}(A\dot{x} - \beta|\dot{x}|z|z|^{\eta-1} - \gamma\dot{x}|z|^\eta) \end{bmatrix} \quad (11)$$

$$\mathbf{B} = [\mathbf{0} \quad \mathbf{I} \quad \mathbf{0}]^T \quad (12)$$

In Equation 11,  $\mathbf{K}$  is the stiffness matrix including the post-elastic stiffness of isolators:

$$\mathbf{K} = \mathbf{K}_{st} + \mathbf{r}_{is}(rk) \quad (13)$$

## 2.2 Natural records analysed

Eight natural records (see Table 3) were chosen from PEER database and, for purposes of comparison, were scaled to the same PGA of 0.25g. Figure 2 shows the acceleration spectra of these scaled earthquakes.

Table 3. Natural earthquakes analysed (PEER database).

Earthquake	Location	Date	M <sub>w</sub>	Distance [km]
Big Bear	California	92/06/28	6.5	45
Superstition Hills	California	87/11/24	6.2	18
Duzce	Turkey	99/11/12	7.1	26
North Palm Springs	California	86/07/08	6.1	42
San Fernando	California	71/02/09	6.6	23
Chi-Chi	Taiwan	99/09/20	6.3	84
Imperial Valley	California	79/10/15	6.5	22
Irpinia	Italy	80/11/23	6.9	10

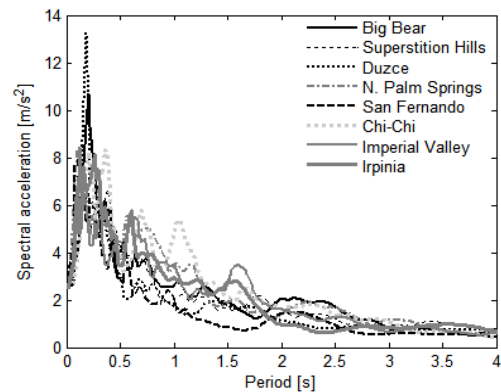


Figure 2. Acceleration spectra of scaled natural records.

### 3 MULTI-OBJECTIVE FVD OPTIMIZATION

#### 3.1 Objective functions

The main function of a damper mounted in an inter-storey isolation system is the reduction of the isolators deflection, and thus of the P- $\Delta$  effects on the substructure. However, as shown in the scientific literature, extra damping may increase the inter-storey drifts and the internal forces in the isolated structure. Therefore, this optimal design aimed at combining the two following competing objective functions (OFs) simultaneously:

- minimisation of the relative displacement of isolation layer OF<sub>1</sub>;
- minimisation of the total drift of superstructure OF<sub>2</sub>.

A limit  $OF_{2,max}$  was assumed for the maximum total drift of superstructure, corresponding to the maximum value reached in the case without FVD. OFs and constraint are shown in Equations 14:

$$OF_1 = \min |d_{iso}^D| = \min |x_3(t) - x_2(t)| \quad (14)$$

$$OF_2 = \min |d_{sup}^D| = \min |x_7(t) - x_3(t)|; \quad OF_{2,max} \leq d_{sup}$$

where  $d_{iso}$  and  $d_{sup}$  are the total drift of isolators and superstructure, respectively, without ( ) or with (D) damper.

In order to obtain a wider range of optimal FVDs, for a more comprehensive assessment of the additional damping, other important structural performance parameters, as storey accelerations and base shear, were only verified as an output of the optimization problem.

In addition to the technical effectiveness, technical feasibility (e.g., maximum deformation of isolation units) and costs must also be evaluated; however, these aspects can be easily verified subsequently for the optimal FVDs obtained, as a wider range of optimal solutions is preferable compared with a few solutions optimizing many objective functions.

The optimal values of the FVD parameters were sought within the following ranges:

- $\alpha$ : from 0.1 to 1.0;
- $c$ : from 1.0 to  $10^7$  N/(s/m) $^\alpha$ .

#### 3.2 Genetic algorithm NSGA-II

The presence of multiple goals in solving a generic problem means that a set of optimal solutions (known as optimal Pareto front) must be obtained, instead of just one optimal solution.

In general, without specific information, none of these solutions can be considered better than another one, and this requires the determination of all possible Pareto-optimal solutions.

To date, many multi-objective evolutionary algorithms are available and effective in determining these multiple solutions in a single simulation run.

Among these algorithms, the fast and elitist Non-dominated Sorting Genetic Algorithm NSGA-II (Deb et al. 2002) has been widely used in practical optimization problems, and it was also chosen for the present study.

The principal parameters set for the application of the NSGA-II algorithm are reported in Table 4; for further details, please refer to Liu et al. (2018).

Table 4. Parameters for the NSGA-II algorithm

Parameter	Value
Number of generations	100
Population size	80
Crossover probability	0.9
Mutation probability	0.1

#### 3.3 Direct optimization procedure

The direct optimization procedure, which is conceptually the simplest one, consists of applying the optimization algorithm directly to the structural response for each single accelerogram analysed.

In particular, time-history dynamic analyses (THAs) of the storey-isolated building were carried out in MATLAB, with a custom-made code, numerically integrating the first-order differential equation of Equation 10 through the explicit Runge-Kutta method.

This code is iteratively called by the optimization algorithm, which is also implemented in a MATLAB code, in order to find the Pareto-optimal solutions. For the candidate solutions ( $c-\alpha$ ), the optimization code prepares the set of FVDs to be evaluated in the dynamic analysis program; then, the latter computes the corresponding time-history responses and the values of  $d_{iso}^D$  and  $d_{sup}^D$  used in the OFs; finally, these values are sent to the optimization code in order to determine the new candidate optimal solutions ( $c-\alpha$ ).

An example of the iterations of the optimization algorithm is shown in Figure 3. The improvement in the solutions is faster for the first generations than for the later ones, where the populations are closer to the optimal Pareto front.

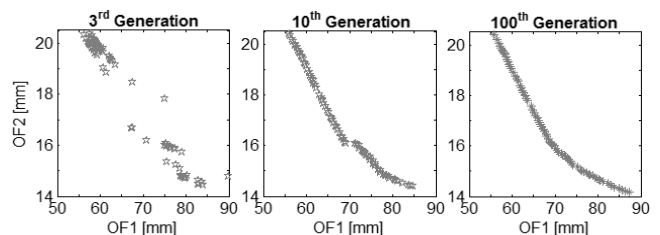


Figure 3. Evolution of the Pareto front for Superstition Hills.

Table 5. FVD parameters ( $c$ ,  $\alpha$ ) and isolators drift ratio between the cases with and without FVD ( $OF_{1,min}/d_{iso}$ ), for the optimal solution  $OF_{1,min}$ .

Earthquake	$d_{iso}$ [mm]	$\alpha$ [-]	$c$ [N(s/m) <sup><math>\alpha</math></sup> ] $\cdot 10^6$	$OF_{1,min}/d_{iso}$ [-]
Big Bear	133.8	0.999	5.095	0.40
Superstition Hills	135.1	0.373	2.283	0.41
Duzce	100.2	0.742	4.028	0.46
North Palm Springs	147.0	0.999	6.560	0.48
San Fernando	88.5	0.718	1.717	0.59
Chi-Chi	122.1	0.100	0.606	0.62
Imperial Valley	130.7	1.000	4.380	0.63
Irpinia	132.8	0.100	0.435	0.71

The overall optimization results, for each earthquake analysed, are reported and commented in the subsequent Section 3.5.

Only for the optimal solution corresponding to the lowest value of  $OF_1$ , i.e.  $OF_{1,min}$ , which minimizes the drift of the isolation system, Table 5 reports the optimal FVD parameters and the associated drift value of the isolators, normalized to the case without FVD, for all earthquakes.

Globally, the reduction in isolation drift achievable in this case study ranges from 30% (Irpinia) to 60% (Big Bear) compared to the case without additional damping, which demonstrates the FVD effectiveness for these applications. However, these optimal solutions refer to  $\alpha$  values (linearity degrees of FVD) that differ greatly depending on the specific earthquake analysed.

Indeed, as discussed in detail in Liu et al. (2018), the  $\alpha$  parameter is strongly influenced by the non-linear seismic response of the structure and, therefore, could depend on the seismic input.

Such a result makes this optimization procedure clearly inappropriate for design purposes, as the  $\alpha$  values (if very different from each other) cannot be averaged.

### 3.4 Optimization procedure based on surrogate response models

In order to overcome the previous issue, a more convenient approach for design purposes consists of applying the optimization algorithm NSGA-II to surrogate response models, rather than directly to the structural response for each accelerogram.

The surrogate response models consist of analytical functions of  $c$  and  $\alpha$  (FVD parameters) that predict the average response of various structural performance parameters (and thus  $OF_1$ ,  $OF_2$ , ...).

In order to derive these surrogate response models, parametric time-history analyses should be carried out evaluating an appropriate number of  $c$ - $\alpha$  combinations within their ranges of interest.

For each structural performance parameter, the maximum values associated with the various accelerograms can be averaged if the number of accelerograms is code-compliant. Then, the peak response surface of that parameter can be obtained by plotting and interpolating its averaged maximum response versus the FVD parameters ( $c$ - $\alpha$  plane). Finally, an appropriate model (generally polynomial, the degree of which should be evaluated case by case) can be calibrated on this peak response surface, and it represents the surrogate response model for that performance parameter.

Therefore, the use of the optimization algorithm with OFs defined on the basis of surrogate response models leads to obtaining overall optimal solutions instead of local optimal solutions, i.e., to a single Pareto front for all accelerograms analysed and hence to the average optimal FVD parameters for the structure analysed.

In general, the output of the surrogate response model can be conveniently normalized to the maximum response value of the relevant parameter in the case without FVD, in order to more directly assess the effects of the additional FVD.

Figure 4 shows the peak response surfaces of the following parameters: drift of isolation layer  $d_{iso}$ , total drift of superstructure  $d_{sup}$  ( $=x_7-x_3$ ), inter-storey drift of the first storey  $x_1$  and absolute acceleration of the top storey  $x_7$ . These response surfaces, which allow to globally assess the effects of additional damping on the structural response, were obtained by linearly interpolating the peak responses associated with all analysed FVDs (indicated with black dots and corresponding to 800 case studies in the range  $c$ - $\alpha$  of interest).

In general,  $d_{iso}$  (Figure 4a) is more influenced by the damping coefficient ( $c$ ) than the damping exponent ( $\alpha$ ), especially for high values of  $c$ ; instead,  $d_{sup}$  (Figure 4b) strongly depends on both the FVD parameters. This is explained by the fact that the reduction of the isolation drift is substantially controlled by the maximum force of the damper rather than by its nonlinearity degree, which instead greatly influences the superstructure response, amplifying the higher vibrational modes in a different way. Furthermore, the two response surfaces of  $d_{iso}$  and  $d_{sup}$  show an opposite or conflicting trend, from which the need for a multi-objective optimization procedure in order to design the best damper solutions.

The trends of  $x_1$  and  $\ddot{x}_7$  (Figures 4 c, d) are quite similar to that of  $d_{sup}$  (Figure 4b), i.e. their value increases with the increase of  $c$  and the reduction of  $\alpha$ , i.e. with the increase of the FVD force and rigidity. Therefore, as already stated, in

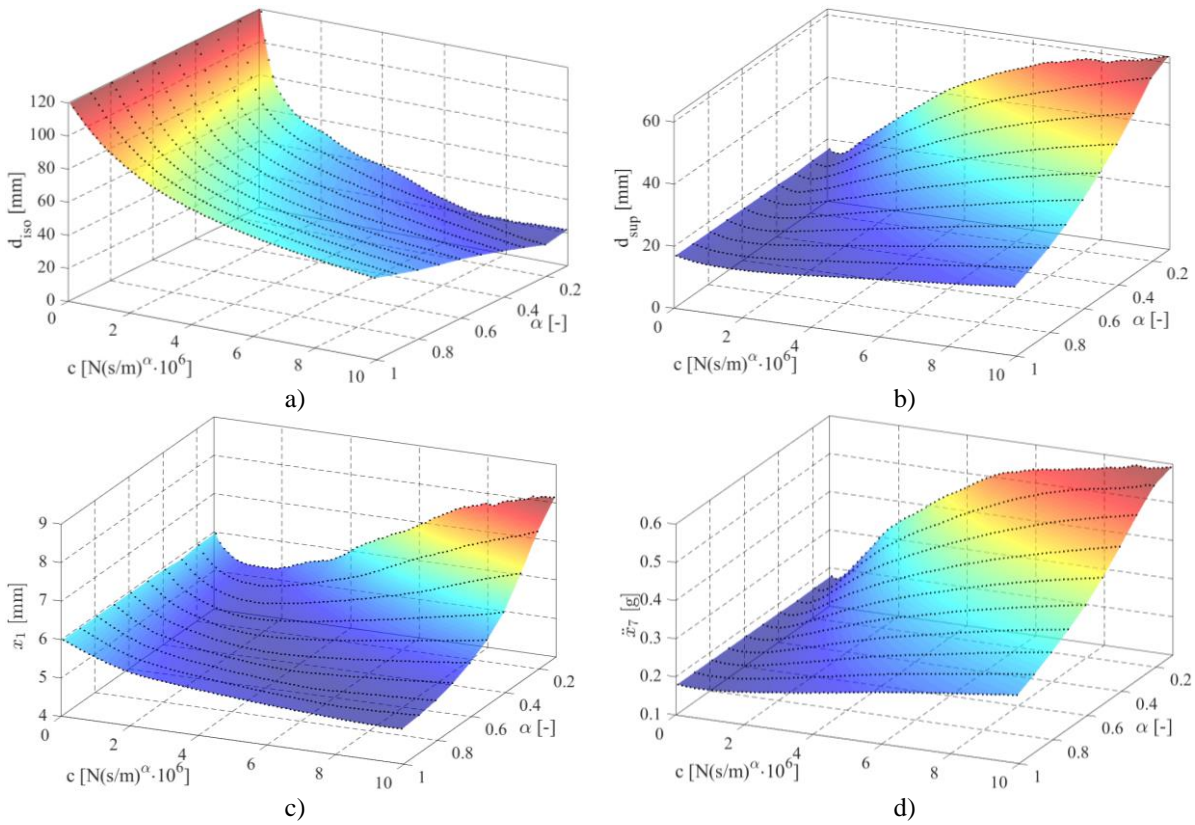


Figure 4. Peak response surfaces: (a) drift of isolation layer  $d_{iso}$ ; (b) total drift of superstructure  $d_{sup}$ ; (c) inter-storey drift of 1<sup>st</sup> storey  $x_1$ ; (d) absolute acceleration of top storey  $x_7$ .

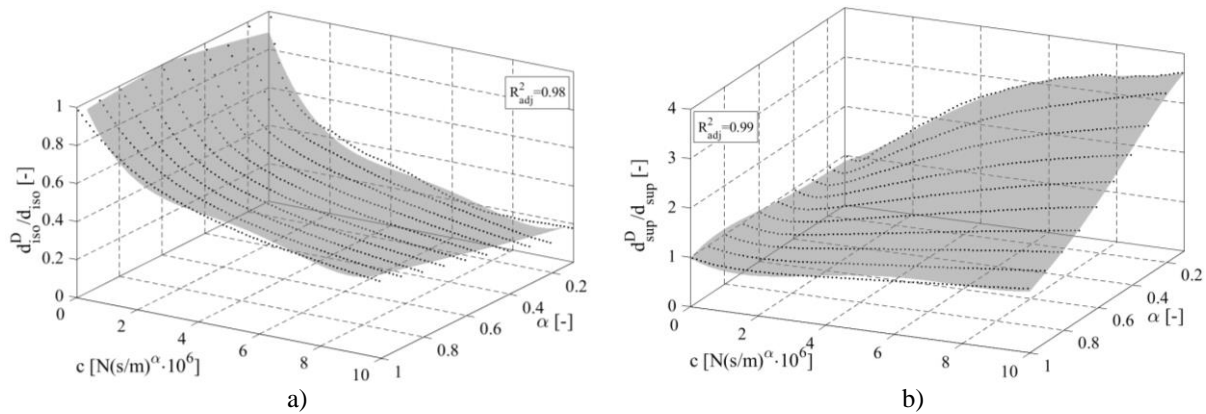


Figure 5. Surrogate response models of  $d_{iso}$  (a) and  $d_{sup}$  (b) normalized to the related maximum response without FVD.

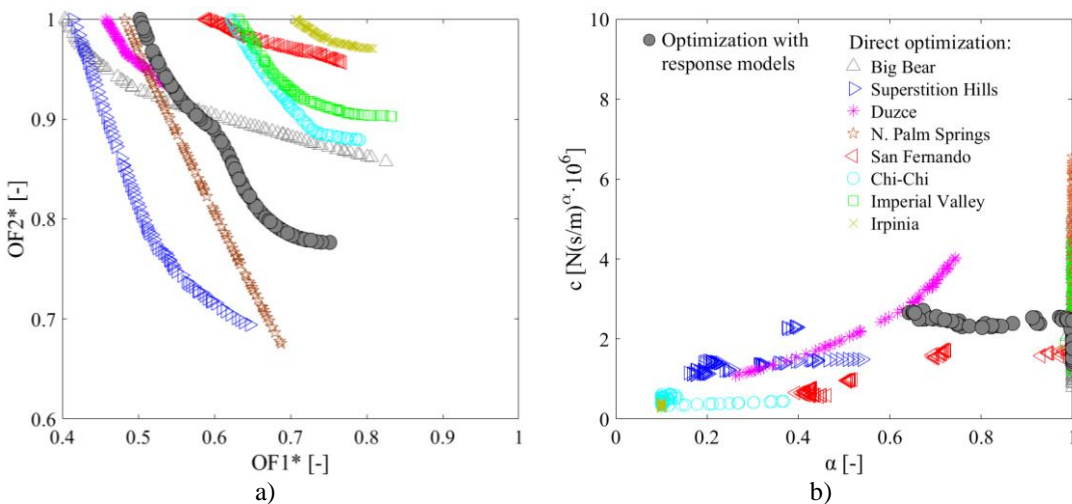


Figure 6. Optimal solutions: (a) values of the objective functions (OF) normalized to the case without FVD; (b) FVD parameters.

order to obtain a wider range of optimal solutions, the values of these additional performance parameters were only verified as an output of the optimization problem (see Section 4.2).

Figure 5 shows the surrogate response models for the parameters  $d_{iso}$  and  $d_{sup}$ , normalized to the relevant maximum value obtained without implementing the FVD. These models, described by the 4-degree polynomial function of Equation 15 and the coefficients of Table 6, allow a good fit ( $R^2 \approx 0.98$ ) compared to the results of the numerical analyses (see Figure 5).

Finally, the optimization results obtained by the simultaneously minimization of these surrogate response models are reported in Section 3.5, and compared with those obtained from the direct optimization procedure.

$$\frac{d_{iso}^D}{d_{iso}} = \frac{d_{sup}^D}{d_{sup}} = b_1 + b_2\alpha + b_3c + b_4\alpha^2 + b_5\alpha c + b_6c^2 + b_7\alpha^3 + b_8\alpha^2 c + b_9\alpha c^2 + b_{10}c^3 + b_{11}\alpha^4 + b_{12}\alpha^3 c + b_{13}\alpha^2 c^2 + b_{14}\alpha c^3 + b_{15}c^4 \quad (15)$$

Table 6. Coefficients of the surrogate response models.

	$d_{iso}^D/d_{iso}$	$d_{sup}^D/d_{sup}$
$b1$	0.8563	0.8642
$b2$	0.3421	0.3819
$b3$	-4.08E-7	4.40E-7
$b4$	-0.2071	-2.1820
$b5$	-4.69E-09	-1.39E-06
$b6$	1.10E-13	6.35E-14
$b7$	0.0468	5.4720
$b8$	5.49E-08	2.03E-07
$b9$	-2.07E-15	1.54E-13
$b10$	-1.35E-20	-1.56E-20
$b11$	0.0806	-3.5580
$b12$	-2.93E-08	4.67E-07
$b13$	-7.77E-16	-8.79E-14
$b14$	7.44E-23	-1.98E-21
$b15$	5.88E-28	7.68E-28

### 3.5 Optimal responses and FVD parameters: comparison between the procedures

Optimal Pareto fronts (in terms of  $OF_1^*$ - $OF_2^*$ ) and associated values of damper parameters ( $c$ - $\alpha$ ) were therefore calculated with both the direct optimization procedure, for each earthquake, and the optimization procedure based on the response models. The main results are shown and compared in Figure 6.

As can be seen in Figure 6a), for some earthquakes (i.e., Big Bear and Superstition Hills) supplemental damping can greatly reduce isolator deflection (with a reduction of up to 60% in this case study,  $OF_1^* \approx 0.4$ ), while ensuring, at most, the same total drift of the superstructure. However, at

other times, this reduction is much lower, indicating that extra damping may sometimes be effective only at the expense of an increase in superstructure drift.

Then, as already anticipated, Figure 6b) clearly shows that the best performance of additional damping can be reached either by linear ( $\alpha \approx 1$ ) or non-linear ( $\alpha < 1$ ) viscous dampers, depending on the specific accelerogram input.

Finally, the optimization procedure based on response models results to be effective in determining the best design solutions for the FVDs, as it provides reasonable and intermediate values, with respect to the direct optimization procedure, both for the optimal Pareto fronts and for the associated FVD parameters.

## 4 EFFECTIVENESS OF OPTIMAL FVDs IN IMPROVING SEISMIC RESPONSE

### 4.1 Building behaviour minimising isolator drift: comparison between the procedures

Although only the total drift of the isolation layer and superstructure were examined as  $OFs$ , other performance parameters should be checked, such as the storey accelerations and the inter-storey drifts. For example, to prevent damage to valuable building contents during an earthquake, a maximum value of storey acceleration is generally assumed according to the type of content, typically about 0.2-0.3g. For some special contents, e.g. artworks or other unique objects, this value may be much lower: however, in this case, specific isolation systems directly applied to the contents are available (Donà 2015, Donà et al. 2017).

Figures 7 a) and b) show, along the building height, the maximum inter-storey displacements and drift ratios (a), and the maximum absolute storey accelerations (b), comparing the cases without FVD (black line) and with FVD (red lines). For the latter case, the optimal damper solution for  $OF_{1,min}$ , which minimize the deflection of the isolation system, was considered. In particular, the results from both the optimization procedures are shown (and for the direct procedure, for all the earthquakes analysed). Figures 7 c) and d) show the same parameters, but normalized to the corresponding values in the case without damper.

These results confirm that additional damping may increase the maximum accelerations and drifts of the superstructure, but also show that this damping is beneficial, in general, for the substructure.

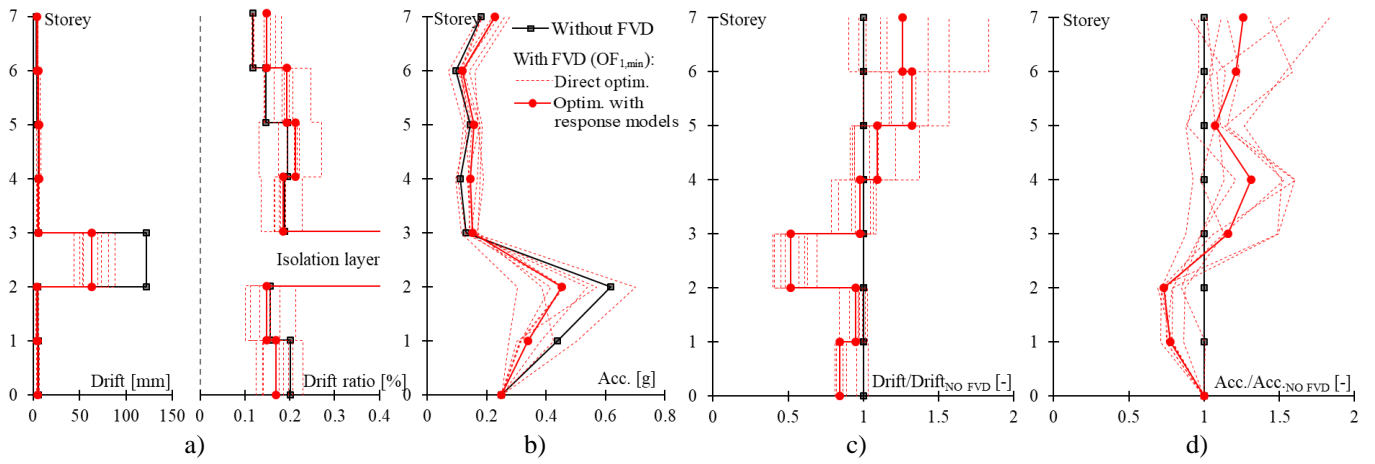


Figure 7. Structural performance, along the building height, without FVD and with the optimal FVD solution for  $OF_{1,min}$ , comparing the results of the two optimization procedures: (a) inter-storey displacements and drift ratios; (b) absolute accelerations; (c), (d) same of (a), (b), normalised to the case without FVD.

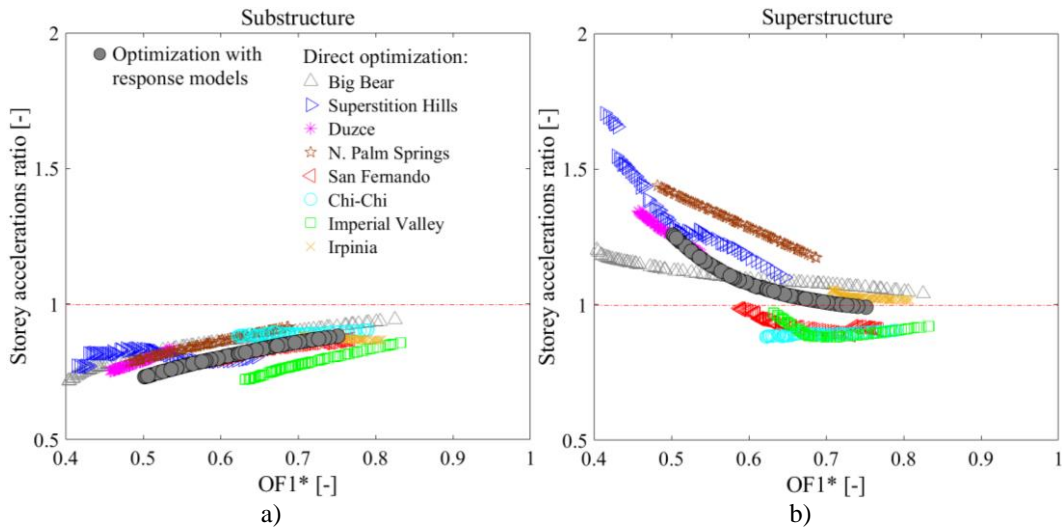


Figure 8. Ratio between maximum storey accelerations, with and without FVD, for (a) substructure and (b) superstructure, versus the drift reduction of the isolation layer  $OF_1^*$  ( $=OF_1/d_{iso}$ ). Comparison between the optimization procedures.

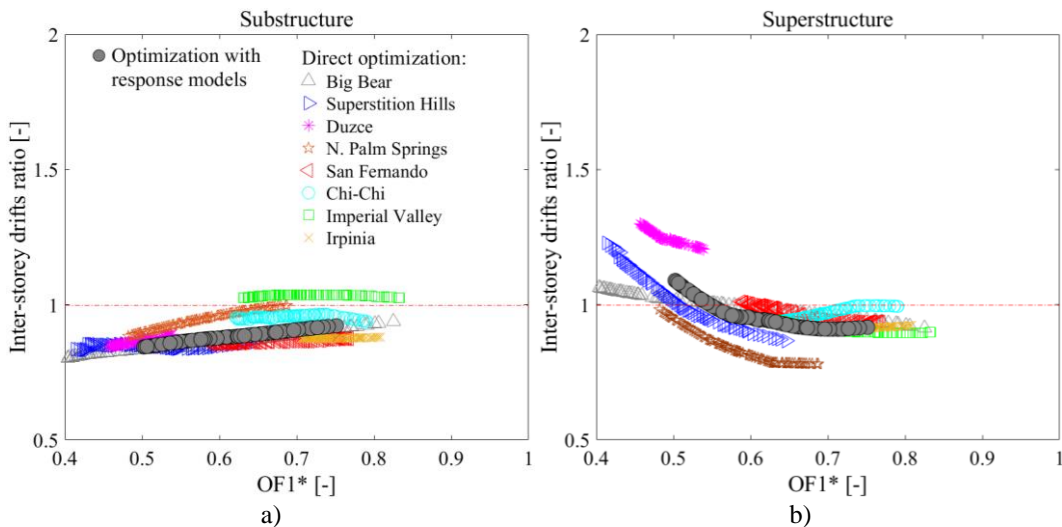


Figure 9. Ratio between maximum inter-storey drifts, with and without FVD, for (a) substructure and (b) superstructure, versus the drift reduction of the isolation layer  $OF_1^*$  ( $=OF_1/d_{iso}$ ). Comparison between the optimization procedures.

In addition, Figure 7 further confirms the effectiveness of the optimization method based on response surfaces, providing an intermediate structural response with respect to those obtained by direct optimization for the various earthquakes.

#### 4.2 Structural performance for all optimal FVDs: comparison between the procedures

Although the amplification obtained for the superstructure response in Figure 7 appears moderate, even in absolute terms, sometimes it may be not acceptable, due to specific design requirements. Since this amplification strongly depends on the amount of supplementary damping (which has the effect of locking the sliding gap offered by the isolation layer), it is interesting to evaluate its trend versus the FVD performance in terms of drift minimisation of the isolation layer ( $OF_1^* = OF_1/d_{iso}$ ), considering all the optimal solutions determined.

Therefore, a comprehensive view of the trend of the ratio between maximum floor accelerations, with and without FVD, for both substructure and superstructure, is shown in Figure 8.

Figure 9, instead, shows the trend of a similar ratio, but examining the maximum inter-storey drifts.

As regards the substructure, both these ratios generally have values lower than 1, together with less influence on damper performance when compared with those of the superstructure. These trends indicate that, if a slightly smaller reduction in isolator drift is accepted, then the highest values of these ratios for the superstructure can effectively be reduced, if they are excessive or in the case of explicit design requirements, without significantly affecting the substructure response.

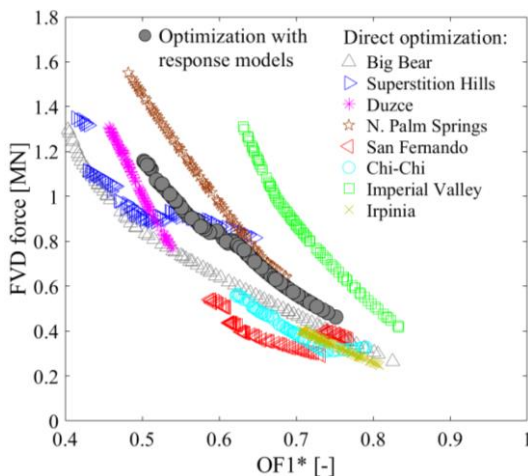


Figure 10. Maximum FVD force versus the drift reduction of the isolation layer  $OF_1^*$ . Comparison between the optimization procedures.

Figure 10 shows the trend of the maximum damper force, which increases more than linearly with decreasing isolator drift ( $OF_1^*$ ). These results are significant and may affect the design choice, as they are closely related to the FVD cost.

Lastly, Figures 8 to 10 also show the effectiveness of the optimization procedure based on response surfaces, providing intermediate results with respect to those obtained by direct optimization.

## 5 CONCLUSIONS

First, this paper presented the main results of a recent research (Liu et al. 2018) about the effectiveness of optimal FVDs in improving the seismic response of a seven-storey building isolated with natural and lead rubber bearings placed between the second and third levels.

In this previous study, a direct multi-objective optimization procedure, which uses the NSGA-II genetic algorithm, is implemented to calculate the optimal values of the FVD parameters for each earthquake analysed. In particular, two competing objectives are simultaneously evaluated, i.e., the minimisation of the drift of the isolation layer and the minimisation of the superstructure total drift.

Among the main results it emerges that the optimal linearity degree ( $\alpha$ ) of an FVD strongly depends on the non-linear structural response, and therefore on the specific seismic input analysed, making the direct optimization procedure not appropriate for design purposes, as it could provide very different  $\alpha$  values for various earthquakes that cannot be averaged.

Therefore, a different approach for the multi-objective optimal design of the FVDs is proposed in this paper and applied to the same case study. This new approach consists in the simultaneous minimization of surrogate response models, which enter into the definition of the OFs. These analytical models, often polynomial, refer to specific structural performance parameters and predict their average peak response between the various accelerograms.

The results obtained from both the optimization procedures are presented and compared. The main highlights are listed below.

- Optimal FVDs allow an effective reduction of the relative displacement of the isolation layer (up to about 50%), while maintaining acceptable maximum values of inter-storey drift and storey acceleration of the superstructure.

- The dynamic response of the substructure is generally improved with optimal FVDs, particularly for high additional damping values (the inter-storey drift of the first storey, thus the total base shear force, can be reduced by about 20%).
- The maximum force developed by optimal FVDs increases more than linearly with decreasing isolator drift; this is an important aspect for choosing the best FVD, as this force affects the damper cost.
- The optimization procedure based on the surrogate response models proved to be effective and more suitable for design purposes.

Although these numerical results depend on the structural configuration of the case study, it is reasonable to believe that the potential shown by FVD systems, optimized to work together with an inter-storey isolation system, is a general result.

## REFERENCES

- Zhang, R., Phillips, B.M., Taniguchi, S., Ikenaga, M., Ikago, K., 2016. Shake table real-time hybrid simulation techniques for the performance evaluation of buildings with inter-storey isolation. *Structural Control and Health Monitoring*.
- Liu, Y.H., Wu, J.B., Donà, M., 2018. Effectiveness of fluid-viscous dampers for improved seismic performance of inter-storey isolated buildings'. *Engineering Structures*, **169**, 276-292.
- Chey, M., Chase, J., Mander, J., Carr, A., 2013. Innovative seismic retrofitting strategy of added stories isolation system. *Frontiers of Structural and Civil Engineering*, **7**, 13–23.
- Zhou, F.L., 2001. Seismic isolation of civil buildings in the People's Republic of China. *Progress in Structural Engineering and Materials*, **3**(3), 268–276.
- Ziyaeifar, M., Noguchi, T., 1998. Partial mass isolation in tall buildings. *Earthquake Eng Struct Dyn*, **27**, 49–65.
- Reggio, A., De Angelis, M., 2015. Optimal energy-based seismic design of non-conventional Tuned Mass Damper (TMD) implemented via inter-storey isolation. *Earthquake Eng Struct Dyn*, **44**, 1623–42.
- Tasaka, M., Mori, N., Yamamoto, H., Murakami, K., Sueoka, T., 2008. Applying seismic isolation to buildings in Japan - Retrofitting and middle-story isolation. In: *Proc. of the 18th analysis and computation specialty conference, ASCE structures congress, Vancouver, BC, Canada*.
- Zhou, F.L., Yang, Z., Liu, W.G., Tan, P., 2004. New seismic isolation system for irregular structure with the largest isolation building area in the world. In: *Proceedings of the 13th world conference on earthquake engineering, Vancouver, BC, Canada*.
- Loh, C.H., Weng, J.H., Chen, C.H., Lu, K.C., 2013. System identification of mid-story isolation building using both ambient and earthquake response data. *Struct Control Health Monit*, **20**, 139–55.
- Kelly, J.M., 1999. Role of damping in seismic isolation. *Earthquake Eng Struct Dyn*, **28**, 3–20.
- Hall, J., 1999. The role of damping in seismic isolation. *Earthquake Eng Struct Dyn*, **28**, 1717–20.
- Providakis, C.P., 2008. Effect of LRB isolators and supplemented viscous dampers on seismic isolated buildings under near fault excitations. *Eng Struct*, **32**, 1187–98.
- Fathi, M., Makhdoumi, A., Parvizi, M., 2015. Effect of supplemental damping on seismic response of base isolated frames under near & far field accelerations. *KSCE J Civ Eng*, **19**(5), 1359–65.
- Ryan, K.L., Polanco, J., 2008. Problems with Rayleigh damping in base-isolated buildings. *Journal of Structural Engineering*, **134**(11), 1780-1784.
- Pant, D.R., Wijeyewickrema, A.C., ElGawady, M.A., 2013. Appropriate viscous damping for nonlinear time-history analysis of base-isolated reinforced concrete buildings. *Earthquake Engineering & Structural Dynamics*, **42**(15), 2321-2339.
- Ismail, M., Ikhrouane, F., Rodellar, J., 2009. The hysteresis Bouc-Wen model: A survey. *Archives of Computational Methods In Engineering*, **16**(02), 161-188.
- Ikhrouane, F., Hurtado, J.E., Rodellar, J., 2007. Variation of the hysteresis loop with the Bouc-Wen model parameters. *Nonlinear Dynamics*, **48**(4), 361–380.
- Donà, M., 2015. Rolling-Ball Rubber-Layer system for the lightweight structures seismic protection: experimentation and numerical analyses. *Ph.D. Thesis*. University of Trento, Department DICAM, Italy.
- Deb, K., Pratap, A., Agarwal, S., Meyarivan, T., 2002. A fast and elitist multiobjective genetic algorithm: NSGA-II. *IEEE Transactions on Evolutionary Computation*, **6**(2), 182-197.
- Donà, M., Muhr, A.H., Tecchio, G., da Porto, F., 2017. Experimental characterization, design and modelling of the RBRL seismic-isolation system for lightweight structures. *Earthquake Engineering & Structural Dynamics*, **46**, 831–853.